JBMR Plus, 2025, **9**, ziaf065
https://doi.org/10.1093/jbmrpl/ziaf065
Advance access publication: April 16, 2025
Research Article

Recombinant ectonucleotide pyrophosphatase/phosphodiesterase 1 (ENPP1) decreases vascular calcification and prevents osteomalacia in a rat model of chronic kidney disease

Kevin O'Brien, Lisa Laurion, Caitlin Sullivan, Jennifer Howe, Angela Malin Lynch[†], Zhiliang Cheng[‡], Denis Schrier, Hervé Husson, Yves Sabbagh[*]

Research and Development, Inozyme Pharma, Boston, MA 02210, United States

[†]Present address: TOXPLUS Monitoring LLC, 677 Citadel Drive, Westmont, IL 60559, United States.
[‡]Present address: Rallybio, 234 Church Street, Suite 1020, New Haven, CT 06510, United States.

[*]Corresponding author: Yves Sabbagh, Research and Development, Inozyme Pharma, 321 Summer Street, Suite 400, Boston, MA 02210, United States (yves.sabbagh@inozyme.com).

Abstract

Chronic kidney disease (CKD) impacts a large percentage of the global population. Chronic kidney disease-mineral bone disorder (MBD) is the broad term describing alterations in key circulating factors involved in mineralization, ectopic calcification, and bone abnormalities. Cardiovascular complications, involving vascular calcification are one of the leading causes of death in this patient population. Plasma levels of pyrophosphate, a potent inhibitor of ectopic mineralization, are low in CKD and end-stage kidney disease patients. These data suggest that the correction of pyrophosphate levels could stand out as a crucial therapeutic goal to mitigate vascular calcifications and reduce cardiovascular mortality. The primary enzyme responsible for the generation of plasma pyrophosphate is ectonucleotide pyrophosphatase/phosphodiesterase 1 (ENPP1). We therefore evaluated INZ-701, a recombinant human ENPP1-Fc fusion protein, in an adenine-induced rat model of CKD. Our investigation revealed that INZ-701 administration resulted in significantly lower levels of calcification in the vasculature and soft tissues. Moreover, INZ-701 treatment significantly prevented the osteoid volume increase observed in vehicle-treated rats, addressing another critical clinical manifestation of CKD-MBD. These results underscore the potential of INZ-701 to reduce vascular calcification and bone mineralization abnormalities in CKD.

Keywords: chronic kidney disease, ENPP1, pyrophosphate, calcification, mineralization, osteomalacia

Lay Summary

As the kidneys shut down, concentrations of minerals such as calcium and phosphate become imbalanced leading to calcification of blood vessels and weak bones. Calcification of the blood vessels leads to cardiovascular disease and is the leading cause of death for those with kidney failure. Here, we describe a rat model of kidney failure that mimics key clinical symptoms. We show that treatment with INZ-701, a drug that prevents genetic forms of vascular calcification and weak bones, reduced calcification of blood vessels and bone abnormalities in a rat model of kidney failure.

Introduction

Chronic kidney disease (CKD) impacts 11%-13% of the global population and ranks as one of the leading causes of mortality worldwide.[1] Chronic kidney disease is divided into stages 1-5 based on the glomerular filtration rate, with stage 5 referred to as end-stage kidney disease (ESKD).[2,3] Chronic kidney disease patients, particularly those in the later stages of the disease, are prone to pathologic and progressive calcification. CKD-mineral bone disorder (CKD-MBD) is a syndrome covering 3 broad categories of abnormal mineralization seen in CKD/ESKD patients: (1) dysregulation of key circulating factors involved in mineralization such as calcium, phosphate, FGF23, vitamin D, and parathyroid hormone (PTH); (2) bone abnormalities including alterations in mineralization and turnover; and (3) ectopic calcification, particularly vascular calcification, a broad definition that encompasses most patients with advanced CKD.[4]

Cardiovascular complications, which may be directly or indirectly linked to vascular calcification, are the primary cause of death in CKD/ESKD patients.[5] Vascular calcification seen in CKD exhibits a high degree of heterogeneity, occurring in both the tunica intima and tunica media of blood vessels, as well as within the aortic valves.[6] The predominant form of vascular calcification in CKD manifests as medial calcification, contributing to increased vascular stiffness and elevating the risk of heart failure and myocardial infarction.[7] The rapid onset of vascular calcification, coupled with the lack of treatment options, highlights the urgent therapeutic need in

Received: November 26, 2024. **Revised:** March 25, 2025. **Accepted:** April 7, 2025

this area.[8–10] Calciphylaxis or Calcific Uremic Arteriolopathy, is a rare condition characterized by calcification in the arterioles and small arteries, resulting in necrotic skin lesions with an estimated incidence of 35 cases for every 10 000 dialysis patients.[11] This disease is predominantly found among ESKD patients, where they often develop sepsis, leading to a mortality rate exceeding 50% within 1 year. Currently, there are no current effective therapeutic or surgical options to prevent or treat calciphylaxis.[12]

Another complication of kidney disease is renal osteodystrophy which refers to bone abnormalities that arise in CKD-MBD and can be classified into high or low bone turnover subtypes.[10] There is considerable variability in the literature regarding the prevalence of the different types of renal osteodystrophy among CKD-MBD patients, with a recent report suggesting that newer treatment regimens are more likely to result in the low-turnover bone disease.[9,10]

The various manifestations of CKD-MBD are interconnected, representing complex interactions among different tissues, signaling pathways, and hormones that have yet to be fully defined. Increased osteoid volume and vascular calcification, for instance, are intertwined, characterized by hypomineralization of bone and simultaneous ectopic mineralization of the vasculature, which is sometimes referred to as paradoxical mineralization.[13] FGF23, through interactions with the FGF receptor 1 and klotho, mediates the downregulation of the phosphate transporters SLC34a1 and SLC34a3, which are expressed in the proximal tubules of the kidney.[14] FGF23 also reduces the concentration of both 1,25 dihydroxy vitamin D and PTH. As CKD progresses, klotho expression decreases.[15] The loss of klotho, coupled with increasing nephrotic damage, impairs FGF23's ability to regulate phosphate levels, which leads to hyperphosphatemia. This is further exacerbated as 1,25 dihydroxy vitamin D levels decrease as the primary location for expression of *Cyp27b1*, the key enzyme required for active vitamin D synthesis, is in the kidney.[16] The loss of active vitamin D results in secondary hyperparathyroidism leading to increased bone resorption and further hyperphosphatemia. FGF23 levels continue to elevate during the progression of CKD. Imbalances in the above hormones, vitamins, and minerals undoubtedly play a key role in both vascular calcification and skeletal abnormalities, but recent work suggests that signaling pathways, most notably the WNT pathway, are also altered, suggesting that factors secreted from sites of vascular calcification can drive mineral bone disease.[17,18]

The paradoxical mineralization seen in CKD-MBD patients is reminiscent of the rare mineralization disorder known as generalized arterial calcification of infancy (GACI), caused mainly by mutations in the ectonucleotide pyrophosphatase/phosphodiesterase 1 (*ENPP1*) gene, known as GACI Type 1, as well as a smaller subset of patients who have mutations in the *ABCC6* gene known as GACI Type 2.[19] Similar to CKD-MBD, patients with GACI Type 1 present with medial vascular calcification and develop osteomalacia in adulthood.[19] Further supporting the connection between this family of disorders and CKD is that mutations in both *ENPP1* and *ABCC6* have been linked to increased vascular calcification in the context of CKD.[20–22] Of note, CKD-MBD, and GACI patients exhibit low plasma pyrophosphate (PPi) levels, where PPi acts as a potent inhibitor of vascular calcification and is generated by the breakdown of ATP by ENPP1.[23–25] In previous studies, PPi levels in dialysis and CKD patients were found to be significantly reduced and inversely correlated with vascular calcification.[25] Additionally, calciphylaxis patients exhibited particularly low PPi levels, which correlated with mortality.[26] We have previously demonstrated that INZ-701 prevents vascular calcification in Enpp1 and Abcc6 deficient mouse models and improves the skeletal phenotype in Enpp1 deficient mice.[27,28] Despite differences in etiology, we propose that the underlying cellular and biochemical mechanisms in these diseases are related to CKD-MBD given the similar disease presentations including low PPi levels, medial vascular calcification, and osteomalacia. Therefore, we evaluated the effects of INZ-701, a recombinant human ENPP1-Fc fusion protein consisting of the catalytic domain of ENPP1 fused to the Fc of human IgG1, in an adenine-induced rat model of CKD-MBD.[27,28]

The model described here recapitulates key aspects of CKD-MBD including reduced kidney function, hyperphosphatemia, medial vascular calcification, osteomalacia, elevated intact FGF23 (iFGF23) and sclerostin (SOST). Treatment with INZ-701 effectively reduced calcification in the iliac arteries, aorta, spleen, and kidney. Furthermore, treatment with INZ-701 was able to significantly reduce the severe osteomalacia observed in this model. These data highlight the potential of INZ-701 as a therapeutic for CKD-MBD.

Materials and methods

Animal model and treatment

CD-IGS Sprague-Dawley (SD) purpose-bred and specific pathogen-free, naïve male rats, at 13-14 wk old were used for this study (SD rats were provided by Charles River Laboratory and performed at Explora BioLabs). Male rats display a consistent pattern of progressive kidney disease development upon adenine administration as described previously as well as the known sex differences in bone biology, which would preclude direct comparison between the sexes.[29,30] Thus, only male rats were enrolled in the study to reduce the total number of animals used in accordance with 3R principles, though future studies utilizing female rats would be of interest to understand any differences between sexes in response to treatment. Animals were acclimated at least 3 days prior to the start of the study and randomly assigned into treatment groups. All animal diets were supplied by Envigo-Harlan Teklad (Inotiv). Animals were fed Teklad Global 18% Protein Rodent Diet (Cat. #2018) prior to the start of the study and changed over to custom diets on day 0 of the study. To induce kidney damage and vascular calcification, we utilized a custom diet made with adenine and lower protein, added calcitriol injections as described previously and established during internal model development as shown in Figure 1. The primary experimental outcome of this study was tissue and vascular calcification. The secondary outcomes were osteoid measurement and plasma biomarkers including PPi, phosphate, and FGF23. Therefore, 6 rats were assigned to the healthy control group, 8 to the CKD vehicle group, and 10 to the CKD INZ-701 treated group based on variation in tissue calcium reported in previous literature and internal model development.[29]

Rats assigned to the healthy control group ("Healthy") received a base diet with a low protein content (low protein diet), 2.5% (TD.200666) for the duration of the study, were administered saline subcutaneously (SC) 3 times a week from day 7 and continuing for the remainder of the study, and PBS

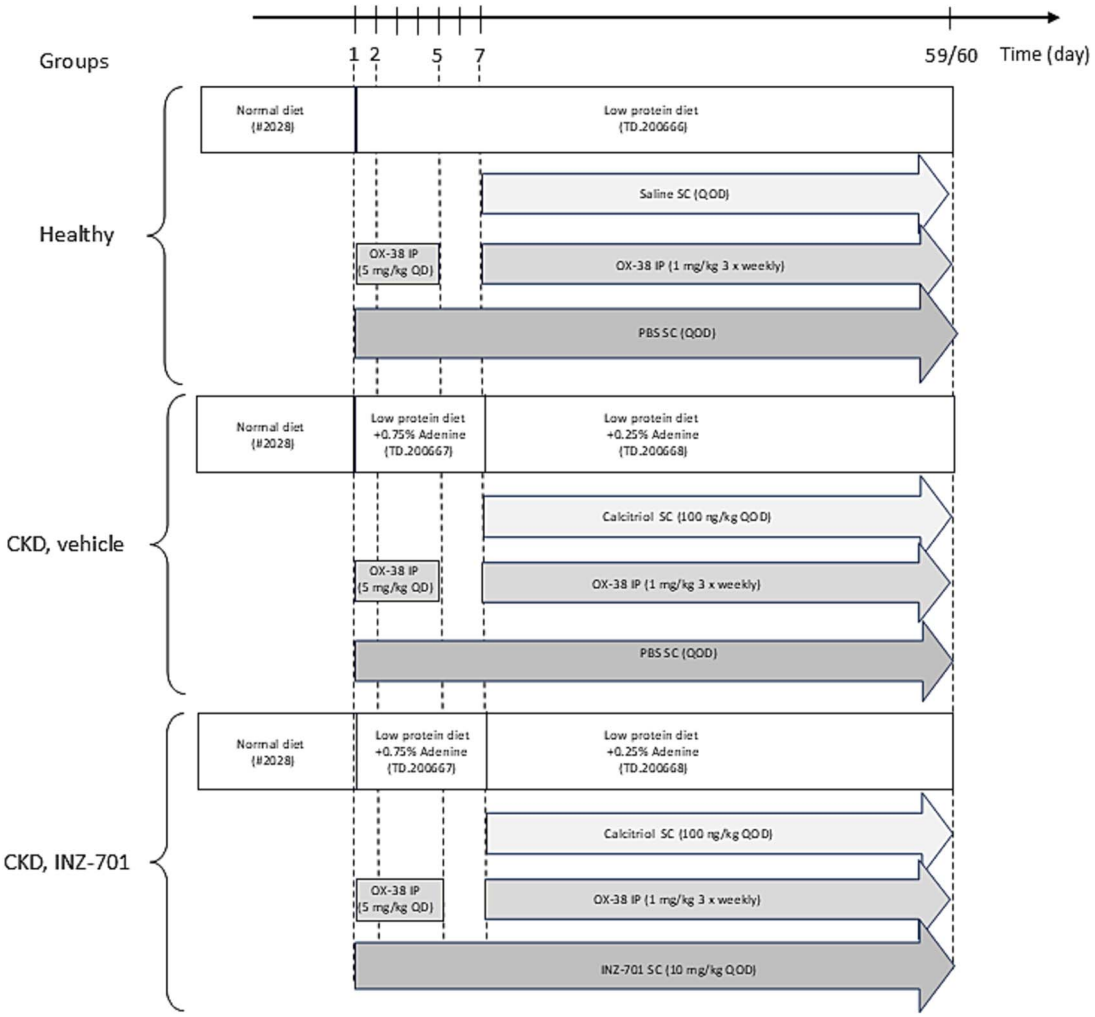

Figure 1. Study design schematic representation. The diets for all rats, with or without adenine, were low in protein. Rats in the healthy group received baseline chow for the duration of the study. Rats in the CKD groups were fed a 0.75% adenine diet for the first week and then switched to a diet containing 0.25% adenine for the remainder of the study. All rats in the CKD groups were dosed with 100 ng/kg of calcitriol beginning on day 7 and dosed every other day (QOD) for the remainder of the study, while the healthy group was dosed with saline vehicle. Rats were dosed QOD with either PBS vehicle or 10 mg/kg of INZ-701 beginning on day 1 of the study. Rats in all groups were dosed with OX-38 to prevent an immune response toward INZ-701. A loading dose of 5 mg/kg was given daily for the first 5 d before a 1 mg/kg dose was given 3 times a week thereafter for the duration of the study.

vehicle SC every other day starting at day 1 and continuing for the remainder of the study. Rats assigned to the CKD groups received a low protein diet +0.75% Adenine (TD.200667) for the first week of the study followed by a change to a low protein diet +0.25% Adenine (TD.200668) with Calcitriol (Cat. #D1530 Millipore-Sigma) administered SC every-other-day at 100 ng/kg beginning on day 7 for the remainder of the study. Immunosuppression, OX-38 (Cat. #BE0308, BioXCell), was administered intraperitoneally at an initial 5 mg/kg daily loading dose from days 1 to 5 and then 1 mg/kg 3 times a week for the remainder of the study and either PBS vehicle ("CKD, vehicle") or 10 mg/kg INZ-701 ("CKD, INZ-701") every other day starting at day 1 and continuing for the remainder of the study. The dose was chosen based on the dose required to completely prevent mineralization as shown in previous rodent calcification models.[27,28] On day 59, 6 animals per group were placed into metabolic cages for the last 22-24 hr of the study while the remaining animals were euthanized by isoflurane overexposure. The rats in metabolic cages were euthanized on day 60. For simplicity, animals euthanized on days 59 and 60 are combined for analysis herein.

All rats were given acidified water (pH 2.5-3.0) ad libitum. Rats were housed in standard disposable caging until transferred to individual metabolic rat cages (Cat. #650-0100, Nalgene) for the last 22-24 hr of the study. When supplementation or hydration was given, all animals, regardless of group, received the same treatment. Hydrogel was offered on the cage bottom following interim bleeds and for the final 3 wk of the study. Nutri-Cal (Vetoquinol) was offered in 1 cm^3 doses/cage, starting at week 2 once/wk, and increasing in frequency to thrice/wk for the final 4 wk of the study. Animal body weights and clinical observations were gathered prior to study initiation and at least twice per week for the duration of the study. These studies were overseen by the Institutional Animal Care and Use Committee at Explora Biolabs (Charles River Laboratories) with full committee protocol amendment review in anticipation of weight loss. Explora Biolabs is an AAALAC, International accredited facility.

Biochemical assays

Processed plasma was analyzed for comprehensive clinical chemistry on an Abaxis VS2 clinical chemistry analyzer for all interim and terminal time points at Explora Biolabs, Inc. Plasma SOST levels in plasma were assayed using the Mouse/Rat SOST ELISA kit (Cat. #MSST00, R+D Biosystems).

ENPP1 activity was measured with a colorimetric assay adapted from assays previously described.[31] Briefly, samples were diluted between 5 and 20 fold in naïve rat plasma to ensure values fall within the assay range (Cat. #RAT00PLLHP2102, BIOIVT) and 10 μL of these diluted samples were incubated at 37 °C with 90 μL of assay buffer (1 M Tris pH 8.0, 50 mM NaCl, 20 μM $CaCl_2$, 20 μM $ZnCl_2$) containing 2 mM pNP-TMP (Cat. #T4510, MilliporeSigma). The production of p-nitrophenol was analyzed kinetically by measuring the absorbance at 405 nm using a SPECTRAmax Plus 384 plate reader (Molecular Devices). The activity was calculated as the change in absorbance over time (mOD/min).

Plasma PPi was measured by a luminescent assay, adapted from assays previously described.[32,33] Briefly, blood was collected at noted timepoints and filtered by centrifugation for 20 min at 14 000 × *g* at 4 °C using a 0.5 mL 50 kDa MWCO filter (Cat. # UFC505096, Amicon) to generate filtered plasma for use in the assay. ATP sulfurylase is used to convert PPi to ATP in the presence of adenosine 5′-phosphosulfate (APS) and ATP levels were then measured using a luminescent assay to obtain total luminescent signals. A standard curve was created by spiking known concentrations of PPi (Cat. #sc251047, Santa Cruz) into water. Filtered plasma samples were mixed with assay buffer (40 mM HEPES pH 7.4, 8 mM $CaCl_2$, 2 mM $MgSO_4$) containing 16 μM adenosine 5′-phosphosulfate (Cat. #A5508, MilliporeSigma), 0.1 U/mL ATP sulfurylase (Cat. #M0394L, NEB). Reactions were incubated at 37 °C for 40 min and followed by 10 min at 90 °C to deactivate ATP sulfurylase. The resulting ATP was then quantified by mixing the reaction mixture in a 1:1 ratio with BactiterGlo detection reagent (Cat. #G8230, Promega). To account for endogenous ATP present in the plasma, a blank reaction was run for each sample with heat-inactivated ATP sulfurylase. The luminescent signals from this reaction were subtracted from the total luminescent signals to calculate the plasma PPi levels.

Tissue calcium was measured in snap-frozen samples including the descending aortae (aortic arch to the diaphragm) and abdominal aortae (to the iliac fork), right common iliac arteries, right kidneys, and spleens. Calcium was extracted from tissues with hydrochloric acid and calcium was quantified with a colorimetric assay using the *O-Cresolphthalein complexone* method as described previously.[34] Briefly, tissues were decalcified in 1 N HCl at room temperature overnight. The acid extract was centrifuged to remove any tissue debris and diluted, as needed, in an additional 1 N HCl. A 5 μL aliquot of sample was incubated with 195 μL of calcium liquicolor reagent (Cat. #0150-250, Stanbio Lab) for 10 min at room temperature. The absorbance of the sample was read at 550 nm using a Molecular Devices SPECTRAmax Plus 384 plate reader. A standard curve for the calculation of calcium concentration was generated in PBS using the calcium reference standard provided in the kit. The tissue calcium content (nmol Ca^{++}/mg) was calculated by converting calcium concentration to mass based on the acid volume and normalized to tissue weight before processing.

Bone imaging

All micro-CT (μCT) scanning was performed and evaluated using Scanco μCT35 (Scanco Medical, AG). An X-ray energy intensity of 55 kV with a current of 114 μA and 300 ms integration time was used. Quantitative analyses were carried out using IPL software (Scanco Medical, AG). Midshaft (cortical) femora were scanned with 12 μm voxels (1024 × 1024 pixels) and 160 slices were used for the evaluation of all 3 groups. The distal (trabecular) femur area was scanned with 12 μm voxels (1024 × 1024 pixels), and 300 slices starting from 250 μm away from the growth plate were used for evaluation.

Histomorphometry

Necropsied femurs were embedded in methylmethacrylate (MMA) and cut in 11 μm sections and placed onto glass slides for Goldner's Trichrome staining to evaluate osteoid measurements. Osteoid measurements were assessed in the distal metaphysis, approximately 250 μm from the growth plate, using an imaging window that captured the majority of the secondary spongiosa in a sagittal section, as outlined in Histomorphometry in rodents.[35] Data were obtained with OsteoMeasure (OsteoMetrics). Two slides per sample were measured at a 50 μm depth difference by 2 different scientists, and the 2 readings were averaged for analysis.

Histology

Necropsied and fixed left kidneys, ascending aortae, left common iliac arteries, and heart tissues were embedded in paraffin, cut in 5 μm sections and placed onto glass slides for von Kossa (Cat. #S1890/S1895/S248 Poly Scientific), or Alizarin Red (Cat. #VB-3008, VitroVivo Biotech) staining as per the manufacturer recommendations. Kidneys were sectioned sagittally to obtain cortex and medullary structures. Aortas and arteries were cross-sectioned to evaluate the medial layers. Hearts were transverse-sectioned to obtain the ventricle walls. Three levels were sectioned from each block. Samples were imaged at 20× with an Axioscan 7 scanning microscope (Zeiss) and stitched together with 10% overlap.

Image analysis

Segmentation and visualization of artery images were performed using the APEER arivis Cloud network AI-based automated image analysis tool (Zeiss).

Aorta images were sorted into 2 classes using the APEER annotation tools. The first class was the aorta or iliac artery, with or without calcification, and the second class consisted of background. After regions were obtained that adequately represented the aorta or artery, the model was downloaded for image analysis in Zen 3.5 (Zeiss). Within the analysis software the aorta or artery automatic segmentation was set with the APEER model, and 2 subclasses of calcification (light brown and dark brown to black), were set with global thresholding. Analysis was completed on 2 to 3 different whole tissue levels per animal, and the mean percent area calcified was calculated.

Statistical methods

All statistical analyses were performed with GraphPad Prism Version 10.4.0. Statistical tests and p values are noted in each individual figure legend. Data are shown as mean ± SEM.

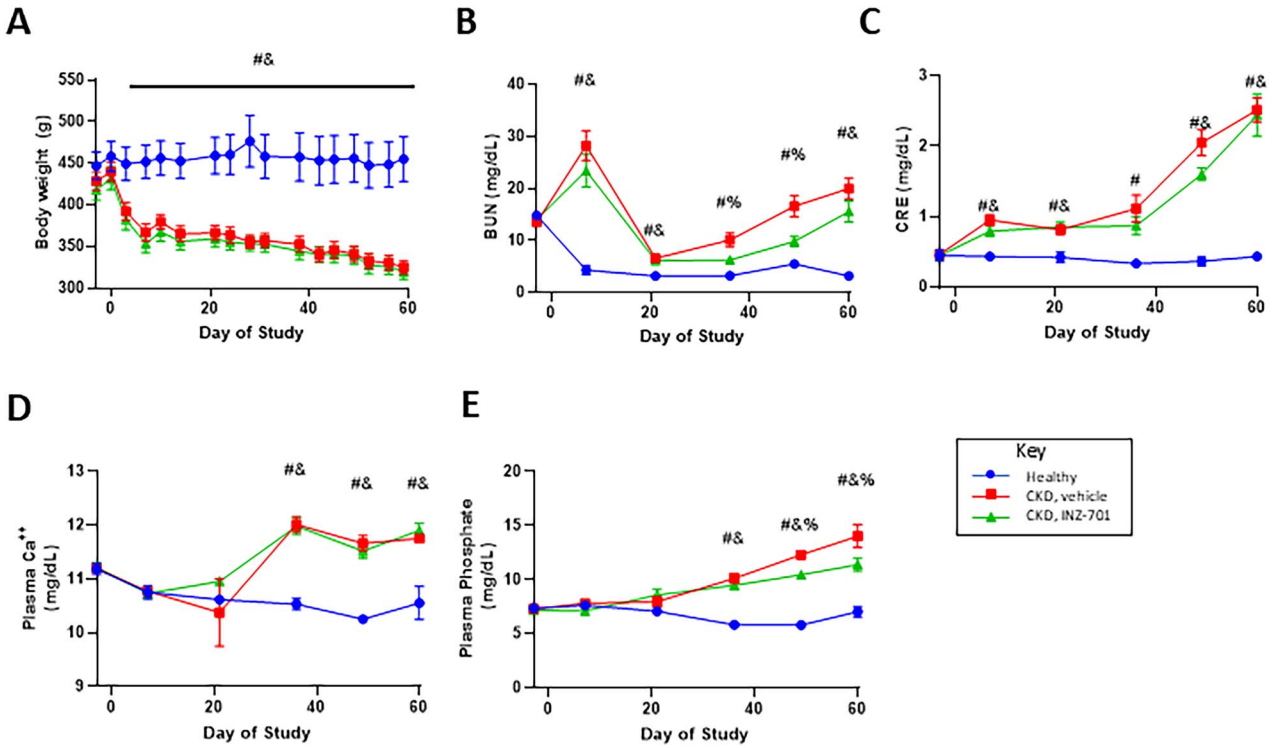

Figure 2. Chronic kidney disease model rats develop kidney damage. Healthy (circles), CKD, vehicle-treated group (squares), and CKD, INZ-701 treated (triangles) groups were analyzed beginning at day −3 to terminal day. Bodyweights are displayed in (A) BUN, in (B) creatinine (CRE), in (C) plasma Ca^{++}, in (D) and plasma phosphate in (E). Ordinary one-way ANOVA used for statistical analysis # indicates significant results ($p < .05$) for healthy vs CKD, vehicle & indicates significant result ($p < .05$) for healthy vs CKD, INZ-701, indicates significant result ($p < .05$) for CKD, vehicle vs CKD, INZ-701. Graphs display mean values and error bars represent ± SEM.

Results

Body weights and plasma chemistry

SD rats fed the 0.75% adenine diet (CKD groups) experienced a precipitous drop in weight relative to the healthy control rats (Figure 2A and Table S1A). By day 7, they exhibited a statistically significant 20% reduction in weight compared to the healthy controls. Following a switch to a 0.25% adenine diet after 1 wk, the rat weights generally stabilized for the duration of the experiment, with bodyweight remaining about 30% lower than those of the healthy group at the terminal timepoint. INZ-701 treatment (CKD, INZ-701) had no impact on bodyweight as compared to vehicle-treated animals (CKD, vehicle). Upon initiation of the 0.75% adenine diet, the blood urea nitrogen (BUN) levels in rats rose approximately 6-fold compared to baseline. After the switch to a 0.25% adenine diet, the BUN levels dropped close to the baseline level and then steadily rose throughout the duration of the study. At the terminal timepoint, BUN levels were 5 times higher in the rats fed adenine diet compared to the rats on baseline diet. Animals dosed with INZ-701 showed slightly lower BUN levels, averaging roughly 15.6 mg/dL, compared to the vehicle-dosed rats, which averaged 20 mg/dL (Figure 2B and Table S1B). After a week on a 0.75% adenine diet, the plasma creatinine levels had doubled compared to the healthy control group. Plasma creatinine levels continued to rise over the course of the experiment, ending at approximately 2.4 mg/dL in the CKD groups compared to 0.4 mg/dL in the healthy group (Figure 2C and Table S1C). Plasma calcium levels were elevated in the CKD groups, averaging 11.8 mg/dL with no impact of INZ-701 dosing, compared to 10.6 mg/dL in the healthy group (Figure 2D and Table S1D). Plasma phosphate levels in the adenine diet groups began to diverge from the healthy group starting at day 21 and slowly elevated throughout the study (Figure 2E and Table S1E). At the terminal timepoint, plasma phosphate in the CKD vehicle group averaged 14 mg/dL, while in the CKD INZ-701, the dosed group averaged 11.4 mg/dL compared to 7 mg/dL in the healthy control group. Thus, plasma phosphate levels are improved by INZ-701 dosing, though the effect is not statistically significant. Plasma alkaline phosphatase, amylase, and albumin were largely unremarkable (Figure S1 and Table S7).

To ensure that INZ-701 maintained drug exposure throughout the study, plasma ENPP1 activity was assessed (Figure 3A and Table S2A). INZ-701 dosed rats show significantly elevated plasma ENPP1 activity levels over the course of the study. iFGF23 levels were significantly elevated in the CKD groups compared to the healthy control group. Chronic kidney disease, vehicle group rats showed average intact FGF23 plasma levels of around 81 000 pg/mL compared to less than 500 pg/mL in the healthy group. iFGF23 levels were lowered to an average of 49 000 pg/mL in the CKD, INZ-701 group, though the effect was not statistically significant due to the heterogeneity of the values (Figure 3B and Table S2C). Sclerostin levels were assessed in the terminal plasma to determine if INZ-701 dosing impacted this important WNT inhibitor (Figure 3C and Table S2C). We found that rats in the healthy group exhibited average plasma SOST levels of 207.4 pg/mL compared to 1309 pg/mL in the CKD, vehicle group. Chronic kidney disease, INZ-701

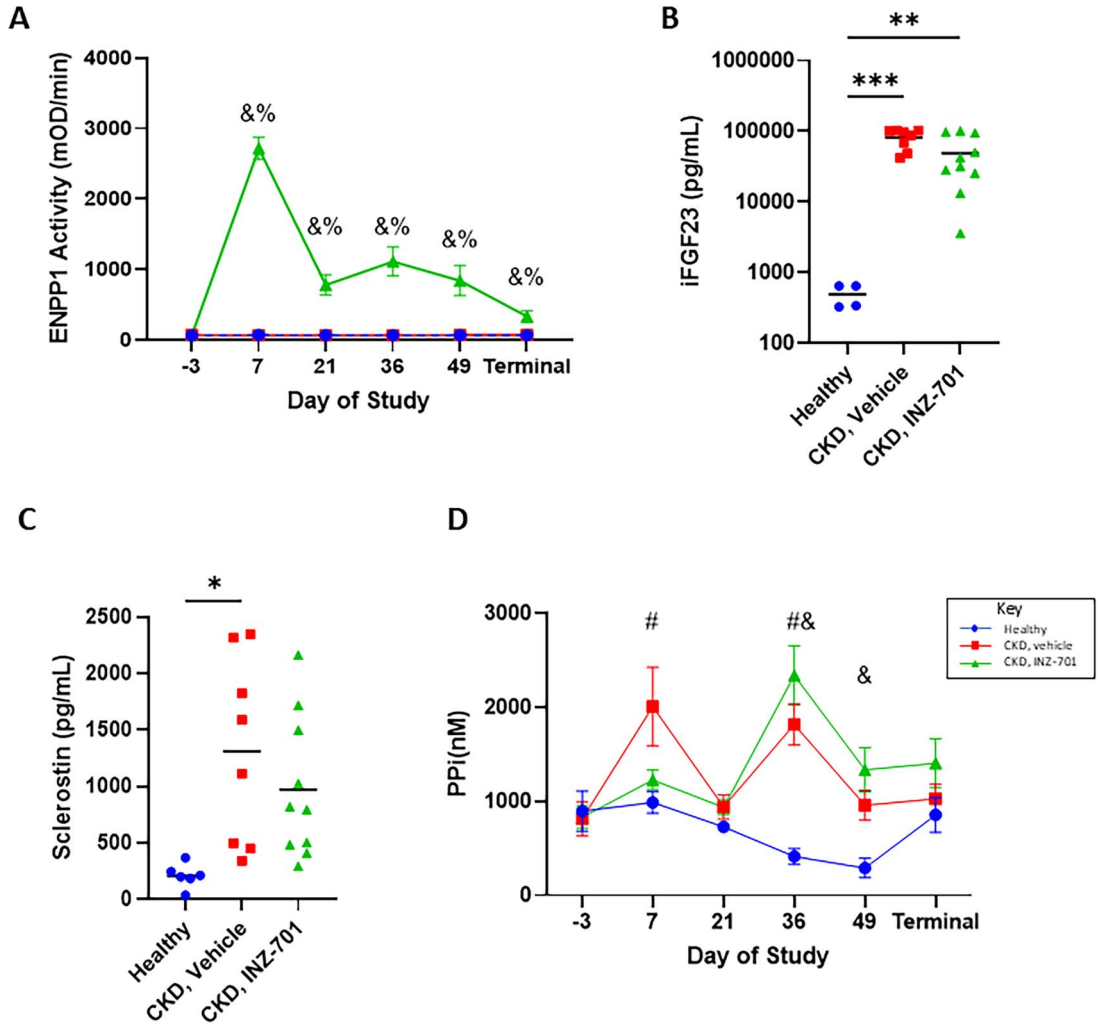

Figure 3. Plasma levels of key biomarkers in CKD model. Plasma biomarkers including (A) plasma ENPP1 activity over the course of the study for healthy (circles), CKD vehicle-treated group (squares), and CKD group treated with INZ-701 (triangles), (B) terminal iFGF23, (C) terminal SOST, and (D) PPi of healthy (circles), CKD vehicle-treated group (squares), and CKD group treated with INZ-701 (triangles). A one-sided unpaired *t*-test was used to assess plasma ENPP1 activity levels, "&" indicates a significant result ($p < .05$) for healthy vs CKD, INZ-701, "%" indicates significant result ($p < .05$) for CKD, vehicle vs CKD, INZ-701. Brown-Forsythe and Welch ANOVA test was used for FGF23 comparison. ***$p = .0001$, **$p = .0065$. Ordinary one-way ANOVA was used for SOST comparison *$p = .0109$. Ordinary one-way ANOVA used for PPi comparison "#" indicates significant result ($p < .05$) for healthy vs CKD vehicle and "&" indicates significant result ($p < .05$) for healthy vs CKD, INZ-701. Horizontal bars on the A-C graphs represent the mean value. The ENPP1 activity and PPi graphs display mean values and error bars represent ±SEM.

rats exhibited a slight reduction in SOST levels, down to an average of 970.1 pg/mL, though the effect was not statistically significant.

Plasma pyrophosphate was assessed at multiple timepoints throughout the study (Figure 3D and Table S2B). Before the start of the study all rats showed equivalent PPi values. However, on day 36, PPi levels were elevated in the CKD group compared to the healthy group. The PPi levels in the healthy group averaged 413 nM compared to 1817.5 and 2341 nM in the CKD vehicle and INZ-701 dosed groups, respectively. PPi levels remain elevated in both CKD groups at day 49 averaging 957.5 and 1336.7 nM in the CKD vehicle- and INZ-701-dosed groups respectively, compared to 292 nM in the healthy control group. By the terminal timepoint PPi levels were equivalent, averaging 855, 1028.8, and 1407 nM in the healthy, CKD-vehicle, and CKD-INZ-701 groups, respectively. It should also be noted that the CKD groups exhibited much higher heterogeneity in PPi levels compared to the healthy control animals over virtually all timepoints except baseline. Interestingly, the divergence of PPi levels in the CKD groups begins at the same point at which phosphate levels begin to increase in these animals, suggesting a global disruption of these pathways.

Calcification

In CKD vehicle rats, von Kossa staining revealed extensive circumferential calcification along the elastic fibers of the iliac arteries and aorta (Figure 4A). Upon treatment with INZ-701, the level of calcium staining in iliac arteries was noticeably lower and image analysis shows a reduction in both light calcification from an average calcified area of 5.47% in CKD animals to 1.59% in CKD animals treated with INZ-701, and dark calcification from an average calcified area of 4.44% in CKD animals to 0.53% in CKD animals treated with INZ-701 (Figure 4B and Table S3B). Iliac arteries from INZ-701 treated CKD rats show an average of 5.2 nmol of calcium/mg of tissue, less than half of the vehicle-treated group, which shows 13.3 nmol of calcium/mg of tissue (Figure 4C and Table S3C).

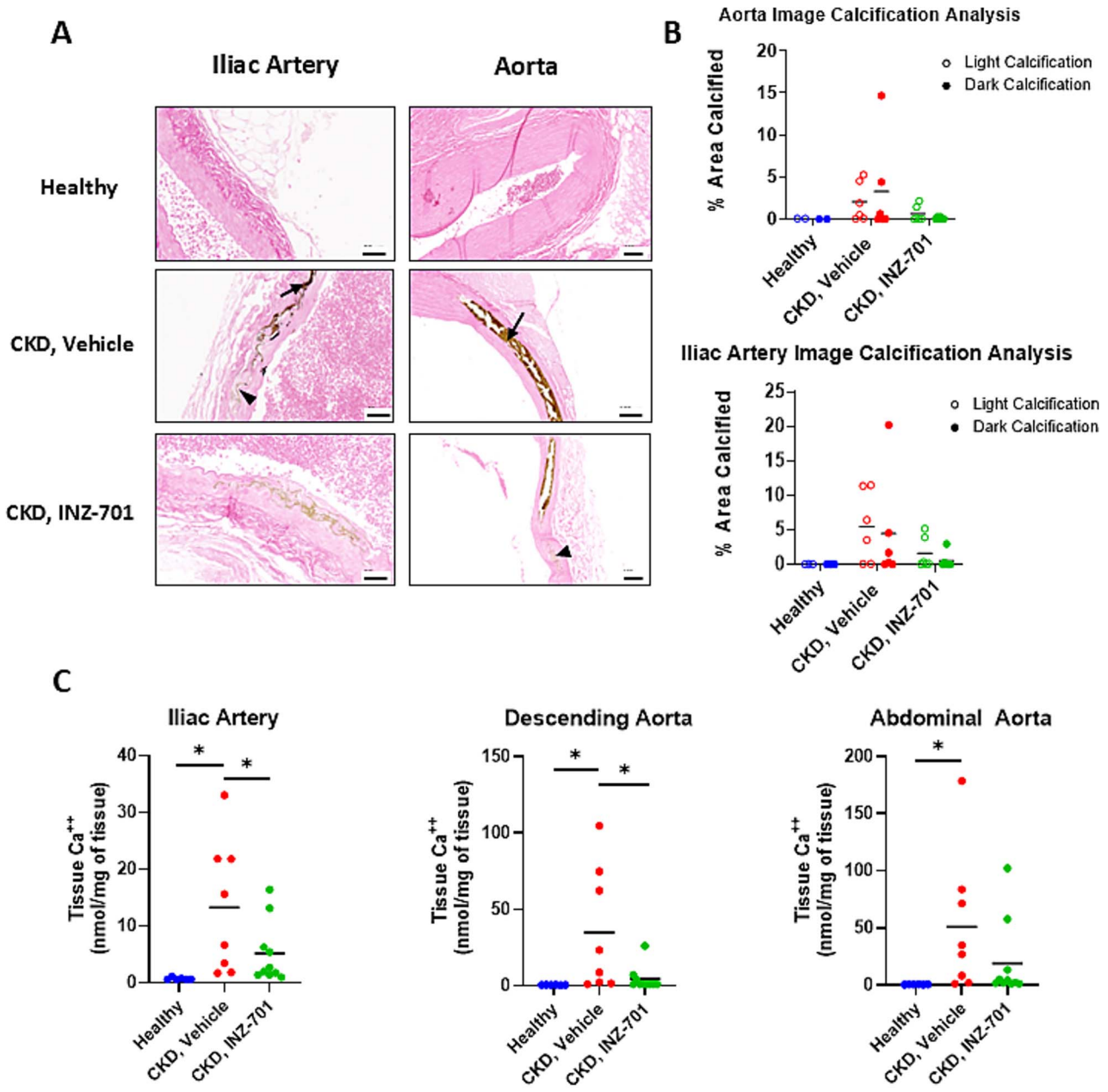

Figure 4. INZ-701 reduces arterial calcification. (A) Representative cross-sections of von Kossa stained iliac arteries and aorta, scale bars: 50 μm (iliac artery, left) or 100 μm (aorta, right). Arrows denote dark mineralization, while arrowheads denote light calcification. (B) Quantification of light and dark calcium deposition. (C) Quantification of total calcium (Ca^{++}) from the iliac artery, descending aorta, and abdominal aorta. One-sided *t*-test. $^{*}p < .05$. Bars on the graphs represent the mean value.

INZ-701 treatment significantly reduced calcification of the descending aorta resulting in 4.6 nmol of calcium/mg of tissue compared to 35 nmol/mg of tissue in the CKD vehicle group. Much the same trend was observed in the abdominal aorta, where mean calcium content was 50.9 and 19.1 nmol of calcium/mg of tissue in vehicle-treated and INZ-701-treated rats, respectively (Figure 4C and Table S3C). Like the observations of the iliac arteries the calcium in the ascending aortas in vehicle treated rats appeared through multiple sections and was often circumferential compared to the more punctate patterns found in INZ-701 treated rats (Figure 4A). Image analysis shows the ascending aortas from INZ-701 treated CKD rats have an average area of less than 1% that is heavily or lightly calcified, noted by the dark and light calcification staining, where the CKD vehicle rats show an average area of 3.30% and 2.06% calcified for heavy and light calcium deposition, respectively (Figure 4B and Table S3A).

Kidneys from CKD rats treated with either vehicle or INZ-701 displayed extensive adenine crystallization and distorted tubules. Alizarin red-stained kidney sections suggested a lower level of calcification in CKD rats dosed with INZ-701 (Figure 5A). To assess kidney calcification, the right kidney was removed at the terminal timepoint and snap-frozen for quantitative calcium analysis. Kidneys from CKD-vehicle-treated rats showed an average of 8.6 nmol of calcium/mg of tissue compared to only 3.2 nmol of calcium/mg of tissue in INZ-701-treated rats (Figure 5B and Table S4). The spleen did show significant calcification in the CKD vehicle group and

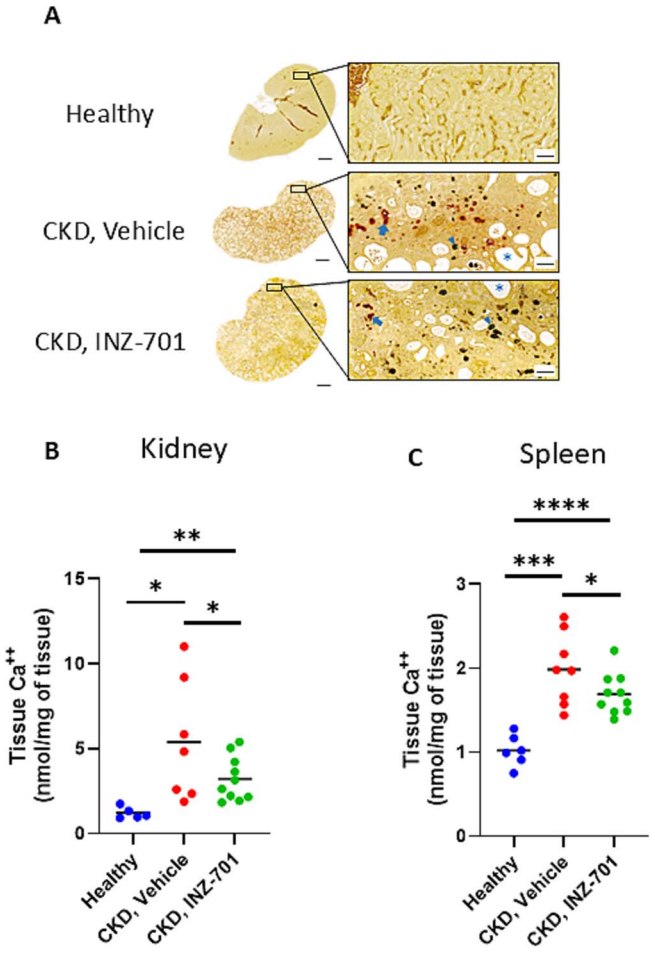

Figure 5. INZ-701 reduces soft tissue calcification. (A) Sagittal sections of the kidney using Alizarin red stain. Brown-black areas are adenine crystals (arrowheads), red staining indicates calcification and is denoted by arrows, and stars indicate distorted tubules. Scale bars: 2000 μm except inset 100 μm. Representative sections of animals with parameters within the average of each group are shown. (B) Quantification of total calcium (Ca^{++}) from kidneys. One-sided *t*-test. $^{*}p = .0136$ (healthy vs CKD, vehicle) and $p = .0477$ (CKD, vehicle vs CKD, INZ-701), $^{**}p = .0026$. The bars on the graphs represent the mean value. (C) Quantification of total calcium from spleen. One-sided *t*-test. $^{*}p = .0401$, $^{***}p = .0001$, $^{****}p < .0001$. The bars on the graphs represent the mean value.

the rats dosed with INZ-701 showed a statistically significant reduction in calcification (Figure 5C and Table S4).

Bone

Bone parameters were assessed via μCT. Micro-CT analyses on both trabecular and cortical bones revealed that the CKD rats had trabecular bone trending towards decreased thickness and spacing with an increase in trabecular number, and there was no impact of dosing with INZ-701 (Figure 6). In contrast, cortical bone in the CKD rats was thinner, with a lower bone area, although not significant for healthy rats. INZ-701 treatment led to an increase in cortical thickness and bone area toward healthy levels, though the effects were not statistically significant (Figure 6 and Table S5).

Histomorphometry

Chronic kidney disease vehicle rats showed a mineralization defect of the femur as measured by Goldner's trichrome-stained femur sections (Figure 7A). The average osteoid area in CKD vehicle-treated rats was significantly increased to 0.29 mm^2 compared to 0.001 mm^2 in the healthy group (Figure 7B and Table S6). The osteoid area in INZ-701 treated rats was statistically indistinguishable from the healthy group, averaging 0.05 mm^2. Osteoid thickness went from an average of 5.9 μm in the healthy rats to 40 μm in CKD vehicle-treated rats. INZ-701 reduced the osteoid thickness to 16.8 μm. Osteoid volume per bone volume went from 0.12% in the healthy control rats to 33.8% in the CKD vehicle group. INZ-701 again restored the osteoid volume/bone volume (OV/BV) to an average of 7.4%, indistinguishable from the healthy group.

Discussion

Chronic kidney disease affects around 850 million people worldwide and presents a major burden on the global health care system.[36] As the disease progresses and patients require dialysis, the dysregulation in mineral metabolism becomes a major contributor to other co-morbidities, such as vascular calcification and renal osteodystrophy, which collectively are referred to as CKD-MBD. The major forms of renal osteodystrophy that have been described are osteitis fibrosa, adynamic bone disease, mixed uremic osteodystrophy, and osteomalacia.[37] The dysregulation of mineral metabolism and bone disease are also driven by pathological changes in key mediators such as FGF-23, TGF-β, SOST, and Dickkopf-related protein-1 the latter 2 of which inhibit WNT/β-catenin signaling pathway.[38–40] The CKD rat model described herein serves as an excellent proxy for CKD-MBD, recapitulating key aspects of the disorder including renal damage, hyperphosphatemia, medial vascular calcification, osteomalacia, and increased circulating levels of iFGF23 and SOST.

Cardiovascular complications are the leading cause of death for CKD.[5] Dosing of CKD rats with INZ-701 prevented calcification of the kidneys, ascending aorta, descending thoracic aorta, carotid artery, and iliac artery. In addition to the quantitative decrease in calcification there is a histological change in the appearance of the calcification. Chronic kidney disease animals dosed with vehicle often show circumferential arterial calcification that extends through multiple histological sections. Animals dosed with INZ-701 show punctate patterns of calcification that do not extend through multiple sections.

The mechanism by which INZ-701 reduces vascular calcification in this model is not clear. We have previously shown that INZ-701 prevented ectopic calcification and prevented bone abnormalities in genetic mouse models that lead to a deficiency in circulating PPi.[27,28] However, in the adenine-induced rat model of CKD studied here, rats had normal PPi levels, suggesting that despite the normal levels of PPi, INZ-701 was able to prevent vascular calcification perhaps increasing PPi concentration in the local environment or potentially manipulating the WNT pathway. These hypotheses are not mutually exclusive.

Although there is a lack of low circulating plasma PPi in our model, the impact of local PPi concentrations on vascular calcification has long been hypothesized but no technique exists to interrogate PPi at a local level.[41] INZ-701 is a soluble form of ENPP1 which can utilize extracellular ATP as a substrate not normally accessible either physically or temporally to endogenous ENPP1 enzyme which is membrane-bound. Access to additional substrate could increase local PPi levels at the sites of vascular calcification

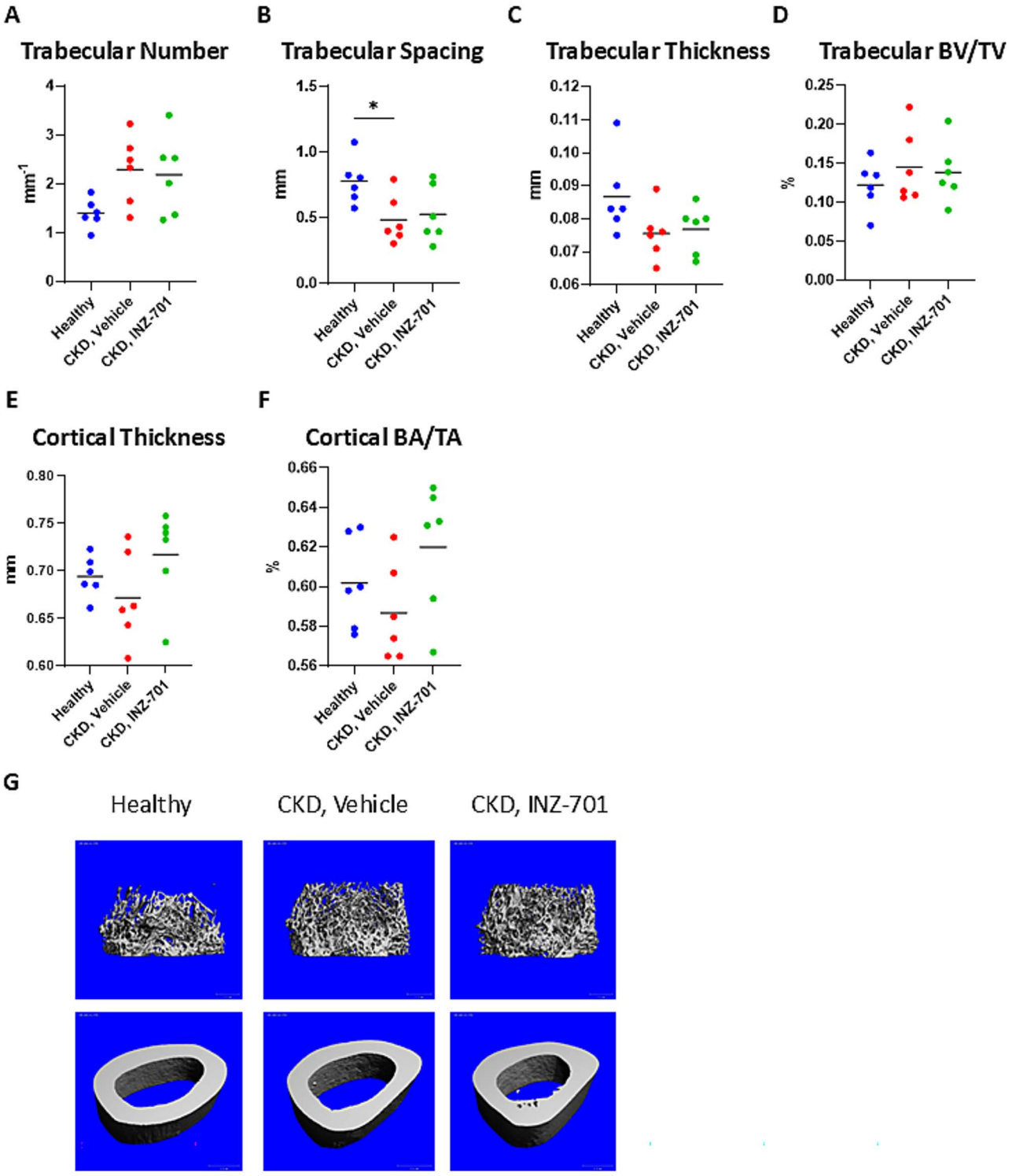

Figure 6. Static bone parameters of femurs. Trabecular number (A), trabecular spacing (B), trabecular thickness (C), trabecular BV/TV (D), cortical thickness (E), and cortical BA/TA (F) were measured. Representative trabecular (top panel) and cortical (bottom panel) images are displayed in (G). Ordinary one-way ANOVA with Tukey's post-test. *$p = .0456$. The bars on the graphs represent the mean value.

preventing progression. The mechanistic reason for low PPi levels in CKD, ESKD, and calciphylaxis patients could be due to disruption of the PPi metabolic pathway. The decreased PPi levels in these patients are not simply an artifact from dialysis, as CKD patients show the same average PPi levels regardless of dialysis status or whether the patient receives hemodialysis or peritoneal dialysis.[25] ENPP1 and ABCC6 are expressed in healthy kidneys; to our knowledge, no data exists on the expression levels of ENPP1 in the kidneys of CKD patients. There is an inverse correlation between circulating ENPP1 level, and calcification of the abdominal aorta in ESKD patients.[42] Mutations in both *ENPP1* and *ABCC6* have been linked to increased vascular calcification in the context of CKD.[20–22]

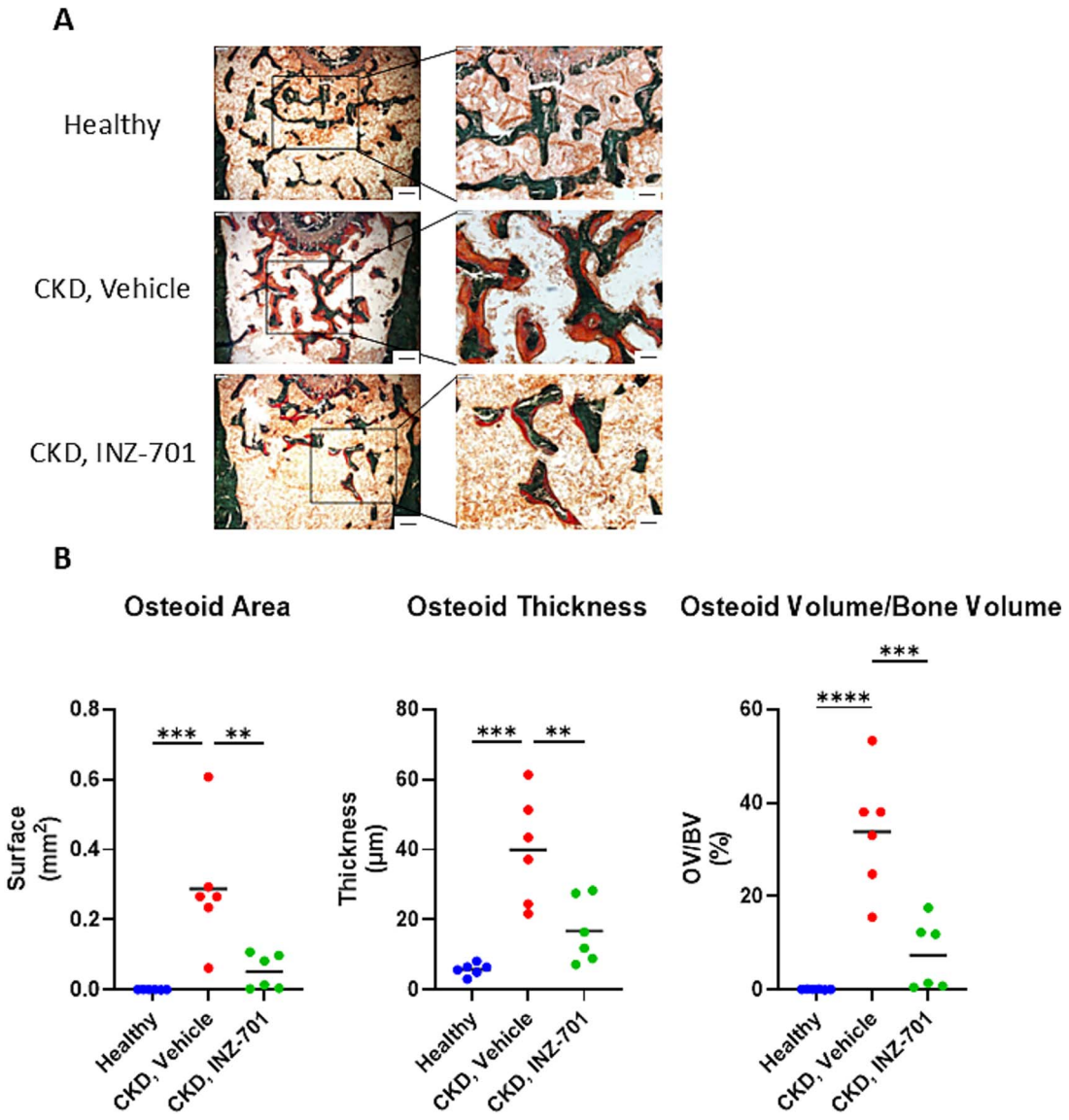

Figure 7. INZ-701 diminishes osteomalacia. (A) Representative images from femurs from rats stained with Goldner's trichrome stain. Dark green: mineralized bone; red: hypomineralized bone/collagen-rich osteoid. Scale bars: 200 μm (left panels); and 100 μm (right panels). (B) Quantification of osteoid parameters, osteoid area: left, osteoid thickness: center and OB/BV: right. Ordinary one-way ANOVA with Tukey's posttest. $^{****}p < .0001$, $^{*}p = .0338$. The bars on the graphs represent the mean value.

Overall, these data highlight the importance of the ENPP1 pathway in decreasing the development of arterial calcification in ESKD patients. ENPP1 activity could be lowered directly in response to pathogenic mutations or indirectly by mutations in CD73 resulting in excess AMP, which inhibits ENPP1.[43] In addition, disruption of CD73 will also lead to lower levels of adenosine which is an inhibitor of tissue nonspecific alkaline phosphatase (TNAP). In either scenario the result would be lower PPi levels. Excess TNAP activity would further decrease circulating PPi levels, suggesting that low PPi levels in these patients may be the result of both lowered production and increased degradation of PPi. In support of this hypothesis, dosing a CKD model mouse with a TNAP inhibitor results in the elevation of plasma PPi levels and partial protection against vascular calcification.[44]

FGF23 is a central regulator of mineral metabolism, FGF23 levels are elevated in CKD patients and rapid elevation is strongly associated with increased mortality. In a recent analysis, CKD patients with slowly rising FGF23 levels were at approximately 4.5-fold higher risk of death compared to patients with stable FGF23 levels and patients with rapidly rising FGF23 levels had about a 15-fold increase in mortality, showing the critical predictive and biological role of FGF23 in CKD pathology.[45] In our model, CKD vehicle rats show a marked elevation in iFGF23 levels over 150-fold higher compared to the healthy group. Hyperphosphatemia is a key driving factor for vascular calcification, as in CKD patients our model rats develop elevated plasma phosphate levels. Dosing with INZ-701 treatment results in a significant decrease in plasma phosphate levels by the end of the study which may partially explain the reduced levels of vascular calcification.

Another aspect of kidney disease is the MBD that also contributes to morbidity. In our CKD model, we observed severe osteomalacia as seen by the significant increase in osteoid area, thickness, and OV/BV in the vehicle-treated CKD rats

compared to healthy rats. INZ-701 normalized the osteoid area and OV/BV to levels that are statistically indistinguishable from healthy rats. Osteoid thickness in INZ-701-treated rats is significantly lower than in the vehicle-treated CKD rats. The striking differences in osteoid size are particularly interesting given the minimal differences between groups in the mineralized bone as measured by μCT. This phenotype is highly reminiscent of the findings in patients with tumor-induced osteomalacia (TIO).[46] In addition, these patients also display high levels of iFGF23 and hyperphosphatemia, like what we observed in the rats described in this study. While the underlying biology of the TIO bone phenotype is not fully understood, it is thought to be the result of high bone turnover disease. Apart from its well-characterized catalytic activity, ENPP1 also acts on the bone through a catalysis-independent mechanism as recently reported.[47] While the elevation of local PPi may explain the prevention of calcification, the prevention of osteomalacia may be the result of this second, PPi-independent mechanism, as one study showed PPi supplementation prevented vascular calcification but not osteomalacia.[48] ENPP1 deficient mice expressing a catalytically inactive version of ENPP1 displayed low PPi levels and developed vascular calcification yet showed largely normal bone parameters compared to vehicle-dosed mice.[47] In the same study, cells from ENPP1 deficient mice showed elevated expression of the WNT inhibitors *Dkk3* and *Sfrp1*. How ENPP1 modulates the WNT pathway is unclear, but we hypothesize that if loss of ENPP1 leads to an increase of WNT inhibitors, then the addition of excess soluble ENPP1 will reduce the levels of WNT inhibitors, resulting in restored bone parameters.

Chronic kidney disease patients show a broad disruption in the WNT pathway with a variety of studies noting an increase in either circulating levels or expression of WNT inhibitors.[38,49] Preclinical models of CKD have noted increases in either expression or circulating concentration of Sfrp1, Dkk1, and SOST.[50] A recent publication suggests that at least some of the circulating WNT inhibitors are derived from sites of vascular calcification and may explain the link between vascular calcification and hypomineralization of bone.[17,18] Consistent with these studies, we note in our current study an increase in SOST levels in our CKD rat model, the levels of SOST trend downward with treatment of INZ-701. Additional studies will be needed to understand the effect of INZ-701 on a broader range of WNT inhibitors as they could have a combinatorial effect on the bone phenotype to understand if this represents a mechanism by which INZ-701 reduces osteomalacia in this model.

While this model recapitulates key elements of ESKD, there are a few shortcomings in our analysis. This model does not result in low circulating PPi levels. Despite the normal PPi levels in the rats, the development of vascular calcification is prevented with INZ-701 treatment. This model, like others of CKD, represents an acute development of the disorder rather than a progressive deterioration of the kidneys. Despite this, we believe the findings of this model are still representative of the clinical disorder given the similarity between phenotypes. While the impact of INZ-701 on this model is dramatic, additional studies will have to be undertaken to understand the mechanism by which it imparts its therapeutic effects in vascular calcification and osteomalacia observed in CKD.

Our study demonstrated that INZ-701 administration prevented vascular calcification and osteomalacia in a rat CKD model suggesting its therapeutic potential in CKD/ESKD patients as well as calciphylaxis patients. These preventative effects suggest that INZ-701 functions by potentially increasing local PPi levels to prevent vascular calcification and modulating the WNT pathway to correct the skeletal pathology observed. Given the importance of PPi in vascular calcification, the protective effect of INZ-701 on vascular calcification may be greater in patients with low PPi.

Acknowledgments

We would like to thank the Bone Analysis Core at UMass Chan Medical School, Worcester, MA, United States.

Author contributions

Kevin O'Brien (Planned study, performed data analysis, and wrote manuscript), Lisa Laurion (Performed data analysis and edited the manuscript), Caitlin Sullivan (Performed data analysis and edited the manuscript), Jennifer Howe (Planned study, performed data analysis, and edited the manuscript), Angela Malin Lynch (Planned study and edited the manuscript), Zhiliang Cheng (Planned study and edited the manuscript), Denis Schrier (Planned study and edited the manuscript), Hervé Husson (Performed data analysis and edited the manuscript), and Yves Sabbagh (Planned study, performed data analysis, and edited the manuscript)

Supplementary material

Supplementary material is available at *JBMR Plus* online.

Funding

All research was funded by Inozyme.

Conflicts of interest

All authors were employees and stockholders of Inozyme at the time these data were generated or analyzed.

Data availability

The data underlying this article will be shared upon reasonable request to the corresponding author.

References

1. Kovesdy CP. Epidemiology of chronic kidney disease: an update 2022. *Kidney Int Suppl*. 2022;12(1):7–11. https://doi.org/10.1016/j.kisu.2021.11.003
2. Levey AS, Coresh J, Bolton K, et al. K/DOQI clinical practice guidelines for chronic kidney disease: evaluation, classification, and stratification. *Am J Kidney Dis*. 2002;39(2 SUPPL. 1):S1–S266.
3. Chen TK, Knicely DH, Grams ME. Chronic kidney disease diagnosis and management: a review. *JAMA*. 2019;322(13):1294–1304. https://doi.org/10.1001/jama.2019.14745
4. Moe S, Drüeke T, Cunningham J, et al. Definition, evaluation, and classification of renal osteodystrophy: a position statement from kidney disease: improving global outcomes (KDIGO). *Kidney Int*. 2006;69(11):1945–1953. https://doi.org/10.1038/sj.ki.5000414
5. Thompson S, James M, Wiebe N, et al. Cause of death in patients with reduced kidney function. *J Am Soc Nephrol*. 2015;26(10):2504–2511. https://doi.org/10.1681/ASN.2014070714

6. Hutcheson JD, Goettsch C. Cardiovascular calcification heterogeneity in chronic kidney disease. *Circ Res*. 2023;132(8):993–1012. https://doi.org/10.1161/CIRCRESAHA.123.321760
7. Jablonski KL, Chonchol M. Vascular calcification in end-stage renal disease. *Hemodial Int*. 2013;17:S17–S21. https://doi.org/10.1111/hdi.12084
8. Kanbay M, Copur S, Tanriover C, et al. The pathophysiology and management of vascular calcification in chronic kidney disease patients. *Expert Rev Cardiovasc Ther*. 2023;21(2):75–85. https://doi.org/10.1080/14779072.2023.2174525
9. Drüeke TB, Massy ZA. Changing bone patterns with progression of chronic kidney disease. *Kidney Int*. 2016;89(2):289–302. https://doi.org/10.1016/j.kint.2015.12.004
10. Dalle Carbonare L, Valenti MT, Giannini S, et al. Bone biopsy for histomorphometry in chronic kidney disease (CKD): state-of-the-art and new perspectives. *J Clin Med*. 2021;10(19):4617. https://doi.org/10.3390/jcm10194617
11. Nigwekar SU, Thadhani R, Brandenburg VM. Calciphylaxis. *N Engl J Med*. 2018;378(18):1704–1714. https://doi.org/10.1056/NEJMra1505292
12. Nigwekar SU, Kroshinsky D, Nazarian RM, et al. Calciphylaxis: risk factors, diagnosis, and treatment. *Am J Kidney Dis*. 2015;66(1):133–146. https://doi.org/10.1053/j.ajkd.2015.01.034
13. Chen Y, Zhao X, Wu H. Arterial stiffness: a focus on vascular calcification and its link to bone mineralization. *Arterioscler Thromb Vasc Biol*. 2020;40(5):1078–1093. https://doi.org/10.1161/ATVBAHA.120.313131
14. Edmonston D, Grabner A, Wolf M. FGF23 and klotho at the intersection of kidney and cardiovascular disease. *Nat Rev Cardiol*. 2024;21(1):11–24. https://doi.org/10.1038/s41569-023-00903-0
15. Li S-S, Sheng M-J, Sun Z-Y, Liang Y, Yu L-X, Liu Q-F. Upstream and downstream regulators of Klotho expression in chronic kidney disease. *Metabolism*. 2023;142:155530. https://doi.org/10.1016/j.metabol.2023.155530
16. Gutierrez O, Isakova T, Rhee E, et al. Fibroblast growth factor-23 mitigates hyperphosphatemia but accentuates calcitriol deficiency in chronic kidney disease. *J Am Soc Nephrol*. 2005;16(7):2205–2215. https://doi.org/10.1681/ASN.2005010052
17. Mace ML, Gravesen E, Nordholm A, et al. Chronic kidney disease-induced vascular calcification impairs bone metabolism. *J Bone Miner Res*. 2021;36(3):510–522. https://doi.org/10.1002/jbmr.4203
18. Mace ML, Gravesen E, Nordholm A, et al. The calcified vasculature in chronic kidney disease secretes factors that inhibit bone mineralization. *JBMR Plus*. 2022;6(4):e10610. https://doi.org/10.1002/jbm4.10610
19. Ferreira CR, Kintzinger K, Hackbarth ME, et al. Ectopic calcification and hypophosphatemic rickets: natural history of ENPP1 and ABCC6 deficiencies. *J Bone Miner Res*. 2021;36(11):2193–2202. https://doi.org/10.1002/jbmr.4418
20. Groopman EE, Marasa M, Cameron-Christie S, et al. Diagnostic utility of exome sequencing for kidney disease. *N Engl J Med*. 2019;380(2):142–151. https://doi.org/10.1056/NEJMoa1806891
21. Schott C, Dilliott AA, Wang J, et al. Vascular calcification in chronic kidney disease associated with pathogenic variants in ABCC6. *Gene*. 2024;927:148731. https://doi.org/10.1016/j.gene.2024.148731
22. Eller P, Hochegger K, Feuchtner GM, et al. Impact of ENPP1 genotype on arterial calcification in patients with end-stage renal failure. *Nephrol Dial Transplant*. 2008;23(1):321–327. https://doi.org/10.1093/ndt/gfm566
23. Rutsch F, Ruf N, Vaingankar S, et al. Mutations in ENPP1 are associated with "idiopathic" infantile arterial calcification. *Nat Genet*. 2003;34(4):379–381. https://doi.org/10.1038/ng1221
24. Lomashvili K, Garg P, Narisawa S, Millan J, O'neill W. Upregulation of alkaline phosphatase and pyrophosphate hydrolysis: potential mechanism for uremic vascular calcification. *Kidney Int*. 2008;73(9):1024–1030. https://doi.org/10.1038/ki.2008.26
25. O'Neill WC, Sigrist MK, McIntyre CW. Plasma pyrophosphate and vascular calcification in chronic kidney disease. *Nephrol Dial Transplant*. 2010;25(1):187–191. https://doi.org/10.1093/ndt/gfp362
26. Chewcharat A, Bouchouari H, Krinsky S, et al. Role of plasma inorganic pyrophosphate in calciphylaxis: a prospective study: TH-OR39. *J Am Soc Nephrol*. 2023;34(11S):12. https://doi.org/10.1681/ASN.20233411S112a
27. Cheng Z, O'Brien K, Howe J, et al. INZ-701 prevents ectopic tissue calcification and restores bone architecture and growth in ENPP1-deficient mice. *J Bone Miner Res*. 2021;36(8):1594–1604. https://doi.org/10.1002/jbmr.4315
28. Jacobs IJ, Cheng Z, Ralph D, et al. INZ-701, a recombinant ENPP1 enzyme, prevents ectopic calcification in an Abcc6−/− mouse model of pseudoxanthoma elasticum. *Exp Dermatol*. 2022;31(7):1095–1101. https://doi.org/10.1111/exd.14587
29. McCabe KM, Zelt JG, Kaufmann M, et al. Calcitriol accelerates vascular calcification irrespective of vitamin K status in a rat model of CKD with hyperphosphatemia and secondary hyperparathyroidism. *J Pharmacol Exp Ther*. 2018;366(3):433–445. https://doi.org/10.1124/jpet.117.247270
30. Diwan V, Small D, Kauter K, Gobe GC, Brown L. Gender differences in adenine-induced chronic kidney disease and cardiovascular complications in rats. *Am J Physiol Renal Physiol*. 2014;307(11):F1169–F1178. https://doi.org/10.1152/ajprenal.00676.2013
31. Jansen S, Perrakis A, Ulens C, et al. Structure of NPP1, an ectonucleotide pyrophosphatase/phosphodiesterase involved in tissue calcification. *Structure*. 2012;20(11):1948–1959. https://doi.org/10.1016/j.str.2012.09.001
32. Jansen RS, Duijst S, Mahakena S, et al. ABCC6-mediated ATP secretion by the liver is the main source of the mineralization inhibitor inorganic pyrophosphate in the systemic circulation—brief report. *Arterioscler Thromb Vasc Biol*. 2014;34(9):1985–1989. https://doi.org/10.1161/ATVBAHA.114.304017
33. Khan T, Sinkevicius KW, Vong S, et al. ENPP1 enzyme replacement therapy improves blood pressure and cardiovascular function in a mouse model of generalized arterial calcification of infancy. *Dis Model Mech*. 2018;11(10):dmm036632. https://doi.org/10.1242/dmm.035691
34. Li T-T, Ebert K, Vogel J, Groth T. Comparative studies on osteogenic potential of micro-and nanofibre scaffolds prepared by electrospinning of poly (ε-caprolactone). *Prog Biomater*. 2013;2:1–13. https://doi.org/10.1186/2194-0517-2-13
35. Erben RG, Glösmann M. Histomorphometry in rodents. *Bone Res Protocols*. 2012;279–303. https://doi.org/10.1007/978-1-4939-8997-3_24
36. Bello AK, Okpechi IG, Levin A, et al. An update on the global disparities in kidney disease burden and care across world countries and regions. *Lancet Glob Health*. 2024;12(3):e382–e395. https://doi.org/10.1016/S2214-109X(23)00570-3
37. Sherrard DJ, Hercz G, Pei Y, et al. The spectrum of bone disease in end-stage renal failure—an evolving disorder. *Kidney Int*. 1993;43(2):436–442. https://doi.org/10.1038/ki.1993.64
38. Graciolli FG, Neves KR, Barreto F, et al. The complexity of chronic kidney disease-mineral and bone disorder across stages of chronic kidney disease. *Kidney Int*. 2017;91(6):1436–1446. https://doi.org/10.1016/j.kint.2016.12.029
39. Liu S, Song W, Boulanger JH, et al. Role of TGF-β in a mouse model of high turnover renal osteodystrophy. *J Bone Miner Res*. 2014;29(5):1141–1157. https://doi.org/10.1002/jbmr.2120
40. Sabbagh Y, Graciolli FG, O'Brien S, et al. Repression of osteocyte Wnt/β-catenin signaling is an early event in the progression of renal osteodystrophy. *J Bone Miner Res*. 2012;27(8):1757–1772. https://doi.org/10.1002/jbmr.1630
41. Ralph D, Levine M, Millán JL, Uitto J, Li Q. Weighing the evidence for the roles of plasma versus local pyrophosphate in ectopic calcification disorders. *J Bone Miner Res*. 2023;38(4):457–463. https://doi.org/10.1002/jbmr.4791

42. Wu X, Di F, Shen S, et al. Levels of serum ecto-nucleotide pyrophosphatase/phosphodiesterase 1 (ENPP1) predicts severity of abdominal aortic calcification in end-stage renal disease patients receiving regular dialysis. *Hemodial Int*. 2022;26(1):23–29. https://doi.org/10.1111/hdi.12969
43. Kato K, Nishimasu H, Okudaira S, et al. Crystal structure of Enpp1, an extracellular glycoprotein involved in bone mineralization and insulin signaling. *Proc Natl Acad Sci*. 2012;109(42):16876–16881. https://doi.org/10.1073/pnas.1208017109
44. Tani T, Fujiwara M, Orimo H, et al. Inhibition of tissue-nonspecific alkaline phosphatase protects against medial arterial calcification and improves survival probability in the CKD-MBD mouse model. *J Pathol*. 2020;250(1):30–41. https://doi.org/10.1002/path.5346
45. Isakova T, Cai X, Lee J, et al. Longitudinal FGF23 trajectories and mortality in patients with CKD. *J Am Soc Nephrol*. 2018;29(2):579–590. https://doi.org/10.1681/ASN.2017070772
46. Schmidt FN, Delsmann J, Yazigi B, Beil FT, Amling M, Oheim R. Approaching virtual osteoid volume estimation and in-depth tissue characterization in patients with tumor-induced osteomalacia. *J Bone Miner Res*. 2024;39(2):116–129. https://doi.org/10.1093/jbmr/zjae008
47. Zimmerman K, Liu X, von Kroge S, et al. Catalysis-independent ENPP1 protein signaling regulates mammalian bone mass. *J Bone Miner Res*. 2022;37(9):1733–1749. https://doi.org/10.1002/jbmr.4640
48. Opdebeeck B, Neven E, Millán JL, Pinkerton AB, D'Haese PC, Verhulst A. Chronic kidney disease-induced arterial media calcification in rats prevented by tissue non-specific alkaline phosphatase substrate supplementation rather than inhibition of the enzyme. *Pharmaceutics*. 2021;13(8):1138. https://doi.org/10.3390/pharmaceutics13081138
49. Pelletier S, Dubourg L, Carlier M-C, Hadj-Aissa A, Fouque D. The relation between renal function and serum sclerostin in adult patients with CKD. *Clin J Am Soc Nephrol*. 2013;8(5):819–823. https://doi.org/10.2215/CJN.07670712
50. Fang Y, Ginsberg C, Seifert M, et al. CKD-induced wingless/integration1 inhibitors and phosphorus cause the CKD–mineral and bone disorder. *J Am Soc Nephrol*. 2014;25(8):1760–1773. https://doi.org/10.1681/ASN.2013080818

JBMR Plus, 2025, 9, ziaf065
https://doi.org/10.1093/jbmrpl/ziaf065
Research Article